ResearchGate

See discussions, stats, and author profiles for this publication at: https://www.researchgate.net/publication/338770864

Morphology-induced fatigue crack arresting in carbon fibre sheet moulding compounds

Article *in* International Journal of Fatigue · January 2020

DOI: 10.1016/j.ijfatigue.2020.105510

CITATIONS
0

READS
45

6 authors, including:



Luca Michele Martulli
Toyota Motor
6 PUBLICATIONS **3** CITATIONS
SEE PROFILE



Soraia Pimenta
Imperial College London
62 PUBLICATIONS **956** CITATIONS
SEE PROFILE



Stepan Lomov
KU Leuven
497 PUBLICATIONS **8,719** CITATIONS
SEE PROFILE

Some of the authors of this publication are also working on these related projects:

M3Strength View project

Multi-scale modeling of the textile materials (FFT vs FEM) View project

All content following this page was uploaded by Luca Michele Martulli on 30 January 2020.

The user has requested enhancement of the downloaded file.

International Journal of Fatigue 2020, 105520
https://doi.org/10.1016/j.ijfatigue.2020.105510

Morphology-induced fatigue crack arresting in carbon fibre sheet moulding compounds

Luca M. Martulli[1,2], Leen Muyshondt[2], Martin Kerschbaum[1], Soraia Pimenta[3], Stepan V. Lomov[2], Yentl Swolfs[2]

[1]Toyota Motor Europe, Material Engineering, Hoge Wei 33, 1930 Zaventem, Belgium

[2]Department of Materials Engineering, KU Leuven, Kasteelpark Arenberg 44, 3001 Leuven, Belgium

[3]meComposites, Department of Mechanical Engineering, Imperial College London, South Kensington Campus, London, SW7 2AZ, UK

*Corresponding author: luca.martulli@toyota-europe.com

Abstract

Carbon Fibre Sheet Moulding Compounds (CF-SMCs) are tow-based composite materials. Interrupted fatigue tests, combined with computed tomography, were performed here to investigate the damage mechanisms in high in-mould flow CF-SMC. The tow-based microstructure created obstacles for fatigue damage propagation, increasing the CF-SMC's resistance against cyclic loading. Failure is shown to nucleate inside the tows, but inter-tow crack propagation tends to be hindered by the presence of the other tows. Tows oriented perpendicularly to the initial fatigue crack stop the crack itself, showing an intrinsic crack arrest mechanism. Additionally, pre-existing manufacturing cracks or voids do not propagate at all. As a result, flatter slopes of the SN diagrams were observed for CF-SMC than for other carbon or glass fibre composites with short, long and even continuous fibres.

1 Introduction

The automotive industry has dedicated an increasing attention to Tow-Based Discontinuous Composites (TBDCs), like Carbon Fibre Sheet Moulding Compound

(CF-SMCs), as a lightweight alternative to metals. CF-SMCs are made of carbon fibre tows dispersed in a partially cured thermosetting resin, forming malleable prepreg sheets. Those sheets are then compression moulded into the desired part. This manufacturing technique enables complex geometries and low cycle times [1].

The static tensile properties of TBDCs are well documented in the literature [2–11]. The stiffness of TBDCs is close to that of Quasi-Isotropic (QI) laminates, while their strength is significantly lower [5–7,9,11]. Both stiffness and strength have shown strong dependency on the compression moulding-induced fibre orientation [5,12].

Significant material heterogeneity has been reported, with significant local equivalent modulus variations in the same specimen [5,7,11,13]. Digital image correlation showed how the final failure usually develops in areas of local lower-than-average stiffness [5,14]. The material hence fails at local strain values ranging from 1.5% to 3%, even though the average failure strain is usually lower than 1% [5,6,11]. The most common failure mechanisms are tow pull-out, tow splitting, tow breakage, inter-tow matrix cracking and tow debonding [2,5,10,11,15].

The minimum lifespan of cars and chassis components must not be compromised by the complex spectrum of load cycles they experience [16]. Therefore, for a widespread industrial use of CF-SMCs, the knowledge of their fatigue response is essential. Despite this importance and the abundance of work on static experimental investigations, very few studies exist on the fatigue of SMCs and TBDCs in general. Selezneva et al. [11] performed a preliminary investigation on the fatigue life of randomly oriented carbon strand thermoplastic. The normalised SN curve was slightly flatter than the one of a QI laminate. This suggests that the discontinuous nature of the reinforcement does not

reduce the durability of the material. Selezneva et al., however, did not investigate whether the difference in slope was statistically significant to claim an improvement in performance.

To the best of our knowledge, no study showed if and how much the tow orientation affects the TBDCs durability. It is known that fibre orientation strongly affects the fatigue behaviour of Short Fibre Reinforced Plastics (SFRP), which are the composites with the most similar microstructure to TBDCs (the main difference being that SFRPs are reinforced by dispersed fibres rather than tows). SFRP specimens with fibres mainly aligned with the load direction have superior durability compared to those with fibres mainly oriented perpendicular to the load direction [17–22]. However, most of the SN curves obtained for different fibre orientations, when normalised, tend to collapse on a single master curve [18,20,23–28]. Whether this holds true for TBDCs as well, remains an open question.

Only a few publications investigated the failure mechanisms of TBDCs under cyclic loading. Mallick [29] investigated the fatigue response of glass SMC. The fatigue damage was attributed entirely to micro-cracks in the matrix. Those reduced the residual static strength significantly. For glass SMC, tow debonding was observed as primary damage mechanism by Larbi et al. [30]. Tang et al. [14] performed tension-tension, tension-compression and compression-compression fatigue tests on CF-SMC, using micrographic investigation to evaluate the damage development. They observed mainly tow debonding and inter-tow matrix cracking. In another study [31], Tang et al. showed how matrix cracking inside or at the edge of the tows is the prevailing damage mechanism in the early stage of the cyclic loading. It was observed that tows oriented

perpendicularly to the load direction tend to develop such cracks earlier. Areas with lower local stiffness are therefore preferential failure site not just in static loading, but also in fatigue loading. Delamination was the main propagation mechanism in [31]. Unlike for the static case, no tow failure was recorded throughout the entire fatigue life of the tested specimens.

These few works do not offer a thorough investigation of fatigue damage propagation in the microstructure of TBDCs. As mentioned earlier, Selezneva et al. [11] noticed similar fatigue performance between a carbon strand thermoplastic and a QI laminate with similar constituent. The authors did not investigate the reason behind such flat slope of the SN curves of the TBDCs, which still remains an important open question.

Tang et al. [14,31] did not investigate extensively the fatigue damage mechanisms. Their work suggests that the damage occurs outside of the tows or on their boundaries, mainly in the form of debonding of matrix cracking. However, the authors did not investigate how each mechanism is involved in the nucleation, propagation and final failure phases. Moreover, the micrographic investigation used suffered from two severe limitations. Firstly, it was destructive, and it was thus not possible to track the nucleation and propagation of individual defects. This hindered the formulation of a possible comprehensive damage development theory. Secondly, the micrographs could only be performed in limited areas and could not analyse the entire specimen volume at the same time. Therefore, a global evolution of the damage evolution within the specimens was impossible to grasp. Overall, a theory that describes the fatigue damage evolution in TBDCs is still lacking.

Finally, all the considered research available for TBDCs considers a planar random tow orientation, as resulting from a low-flow moulding. As mentioned earlier, this implies that the effects of the tow orientation on the fatigue performance of TBDCs are not known.

Recently, X-ray micro-Computed Tomography (µCT) has been used, in combination with cyclic loading, to characterise the fatigue damage mechanisms in composites [32]. Two common approaches are *in-situ* µCT, in which the scanning is performed during the loading, or *ex-situ* µCT, in which the load is interrupted to allow the specimen to be scanned. *In-situ* techniques might give a deeper insight on the damage evolution, but also come with several limitations. Garcea et al. [32] highlighted that when significant amounts of cycles are considered at low frequency (5 Hz), *in-situ* investigations become impractically long. Moreover, they often require synchrotron radiation. Garcea et al. [33,34], for example, were able to perform an in-situ investigation for a total of 800 cycles, only 100 of which were actually scanned with the synchrotron radiation. *Ex-situ* techniques, on the contrary, do not limit the number of cycles that can be applied between scans. In addition, any µCT lab equipment can be used, making the experimental campaigns more flexible, faster and cheaper. The damage evolution mechanisms are not as easy to identify as in the *ex-situ* techniques; nevertheless ex-situ techniques have been successfully used on composites in combination with fatigue loading [32,35,36].

This study investigates the relations between the CF-SMC microstructure and their fatigue performance through the use of ex-situ µCT. Specimens subjected to tension-tension fatigue were therefore scanned with µCT before the first fatigue cycle, at

intermediate number of cycles and after failure. The technique was applied to a CF-SMC material at different directions relative to its prevailing orientation.

2 Materials & methods

2.1 Materials and production

The material used to manufacture the plates was STR120N131 from Mitsubishi Chemical Carbon Fiber and Composites GmbH's [37]. It is made of a vinyl ester matrix, and a 42% volume fraction of carbon fibre TR50S [38] tows. Tensile strength and modulus of the fibres were 4900 MPa and 240 GPa, respectively. The fibre count of the tows was 15K, while their nominal dimensions were 25.4 mm x 8 mm x 0.115 mm. Table 1 reports details on the fibres, as provided by supplier.

Table 1: Properties of the dry fibres [38]

Strand Tensile Strength	Strand Tensile Modulus	Elongation	Fibre diameter
4900 MPa	240 GPa	2.0%	6.8 μm

Plates with dimensions of 458 mm x 458 mm x 2.5 mm were compression moulded with a moulding temperature, pressure and time of 141.5 °C, 215 bar and 180 s, respectively. The prepreg sheets occupied only 20% of the mould cavity, as shown in Fig. 1a. The consequent in-mould flow is known to reorient the tows along the flow direction (Fig. 1b). Finally, specimens of dimension 250 mm x 25 mm x 2.5 mm were waterjet cut forming an angle of 0°, 45° and 90° with respect to the prevailing flow direction (Fig. 1c, Fig. 1d and Fig. 1e, respectively). For the rest of this paper, they will be referred to as "0°", "45°" and "90°" specimens, respectively. In Fig. 1, the coordinate

system that will be used throughout this work is also shown. More details on the manufacturing procedure are reported in [5].

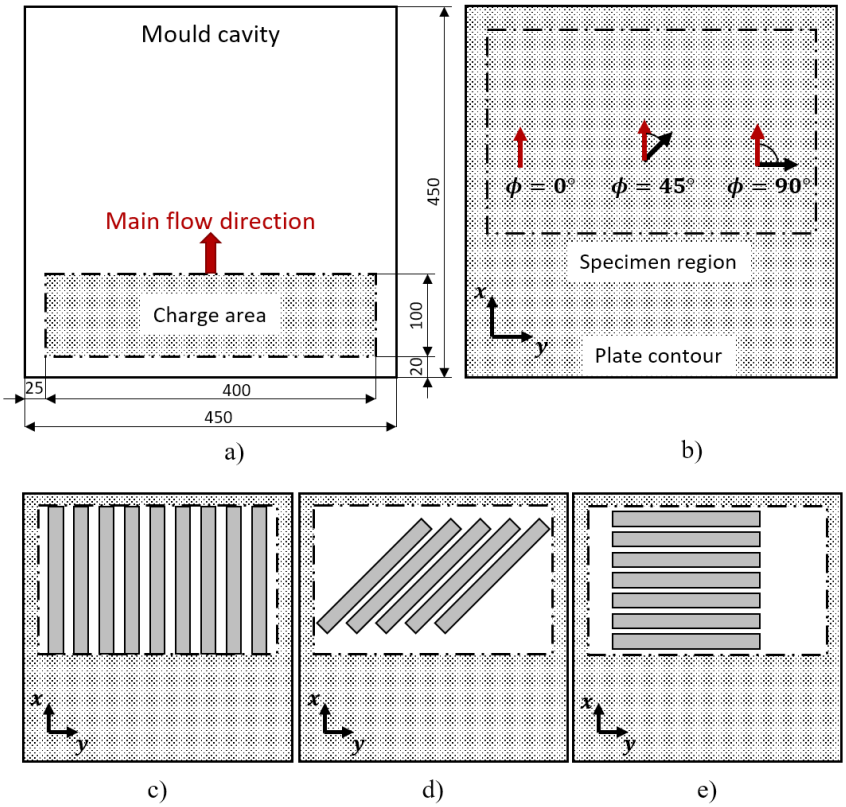


Fig. 1: Oriented specimens manufacturing: a) plate manufacturing scheme and b) induced orientation. Scheme for cutting the specimens at c) 0°, d) 45° and e) 90°.

2.2 Fatigue tests

The tension-tension cyclic tests were performed following the ASTM D3479 standard [39]. The gauge length of the specimens was 150 mm. Two machines were used for the tests: the 0° and the 90° specimens were tested on a Combined Schenk, with a 160 kN load cell; the 45° specimens were tested on an Instron 8872 with a 25 kN load cell. The use of two different machines helped speed up the testing campaign. This does not introduce any difference in the resulting SN diagram, since the specimens failing near the grips were discarded.

The load was applied as a sinusoidal wave shape. The stress ratio R of the nominal minimum to nominal maximum applied stress was 0.1. SN curves were constructed by registering the number of cycles to failure and the nominal maximum stress for each specimen. Samples not failing after 10^6 cycles were considered as run-out tests. The load levels considered were chosen as fractions of the Ultimate Tensile Strength (UTS) measured in [5].

The frequency of the cyclic load had to be selected to avoid an increase of the temperature of the specimens of more than 10°C. For this reason, thermocouples were attached on a 90° specimen tested, which was considered the worst orientation in terms of heating up. The specimen lasted 10^6 cycles at 5 Hz frequency, and fluctuations of less than 3°C around room temperature were measured. The frequency of 5 Hz was thus selected for all tests.

2.3 X-ray micro-CT

A GE Nanotom X-ray micro-CTsystem was used to perform the µCT analysis. Voltage and current were 60 kV and 290 mA, respectively. The voxel resolution was set to 12.5 µm. The entire gauge length of two 0° and two 90° specimens was scanned before testing by scanning and merging 5 consecutive volumes. Only the failure section was scanned after breaking. Several intermediate scans of the entire gauge length were also performed. The specimens used for this analysis were not included in the SN curves.

3 Results

3.1 SN curves

Fig. 2a shows the logarithmic SN curves obtained from the fatigue tests, showing a clear linear trend. The static UTS reported in [5] are included to facilitate comparison. The trendlines reported were constructed by excluding both the static tests and run-outs. A linear fit of the considered point led to the equations reported in Fig. 2. The number of valid points for the 0°, 45° and 90° cases were 16, 10 and 10, respectively. In addition to those, one run-out specimen was found for the 0° case, and three for the 45° and 90° cases.

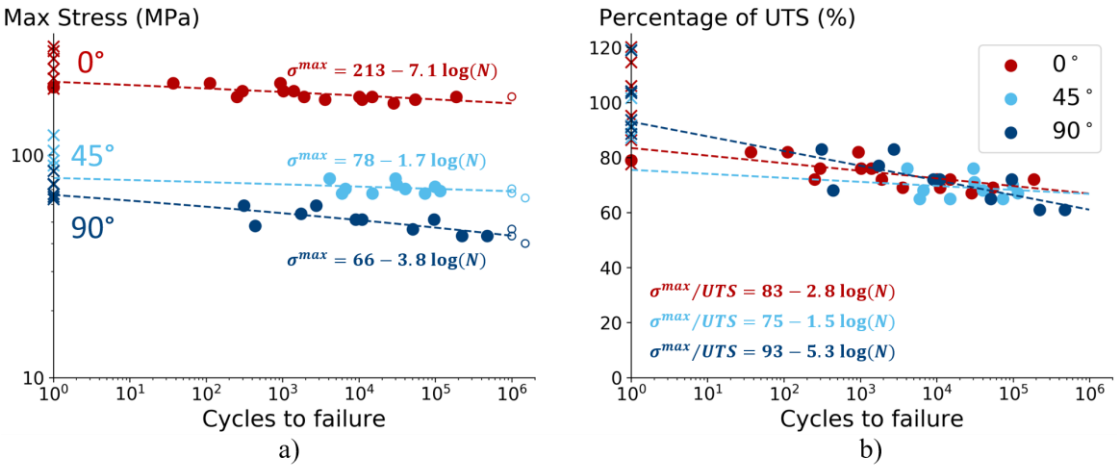


Fig. 2: SN curves in terms of a) maximum applied stress (logarithmic scale) and b) percentage of UTS (semi-logarithmic scale). Crosses indicates static tests.

The curves are normalised in Fig. 2b. This was done by dividing the maximum applied stress of each specimen with the average UTS of that specimen's orientation group. Interestingly, the scatter in the fatigue data seems to be much smaller than that of the static data.

Note that one 0° specimen failed in the very first cycle. This is caused by the high scatter observed in the UTS: for particularly weak specimens, 80% of the average UTS may be too close to its actual UTS.

An ANOVA analysis with a 95% significance level was not able to prove that the normalised fatigue strengths belong to different populations. The analysis was performed as instructed in [40,41]. This suggests that tow orientation has only a minor effect on the normalised SN curves.

3.2 Failure behaviour

Fig. 3 shows typical pictures of the fracture profiles of one specimen per group. The fracture profile of statically broken specimens, as reported in [5], are included for comparison. Both load cases clearly show an influence of the global preferential orientation on the fracture profile of the specimens. The 0° profiles have a very irregular surface, because of the many pulled out tows. The 45° and 90° have smoother fracture surfaces, that follow the prevailing orientation. More pulled-out tows seem to be present in the fatigued 0° specimen than the static one. Apart from this small observation, it is not possible to distinguish between a fatigued and a statically broken sample.

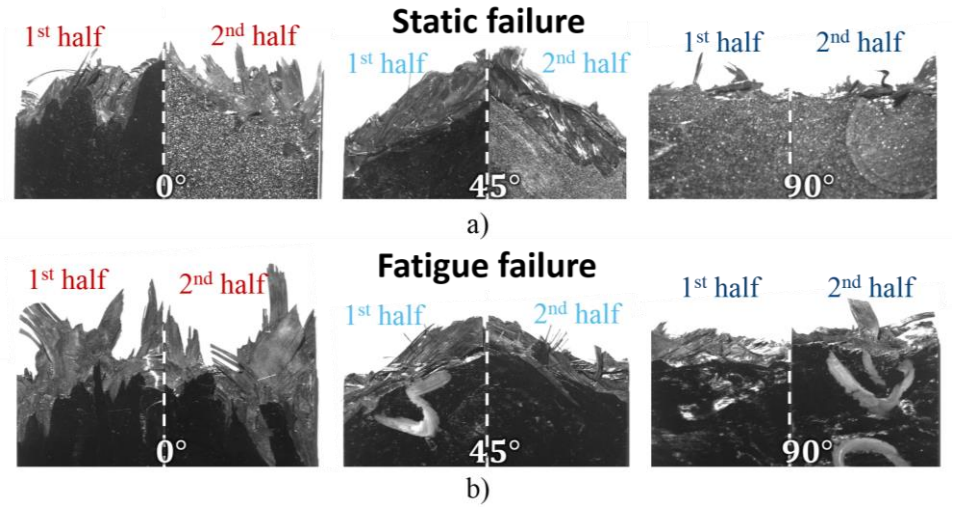


Fig. 3: Fracture profiles of a) static and b) fatigued samples, at different orientation.

Fig. 4 sums up the strategy adopted for the µCT investigation during interrupted testing, and shows the naming system.

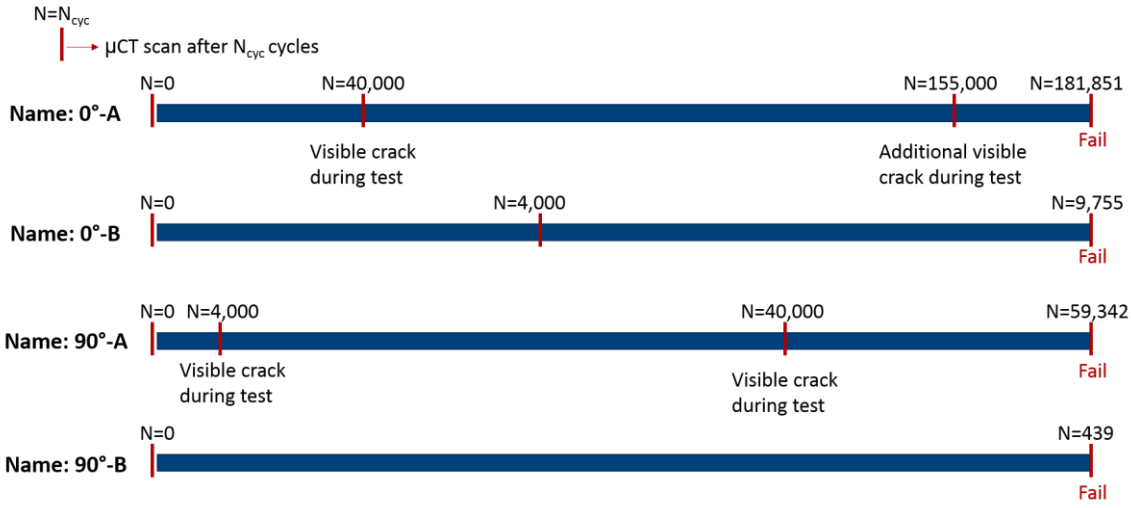


Fig. 4: µCT investigation overview

Fig. 5 shows the evolution of a crack in the 0°-A specimen, which was not present before the test. In the 40k scan, the crack only exists inside a tow (see Fig. 5a), proving that this crack nucleated as an intra-tow feature. The intra-tow crack follows the fibre orientation, and its smooth nature indicates no fibres are broken. In the 155k scan, the intra-tow crack is found to propagate outside the tow in the negative z-direction. First it

spreads through a similarly oriented tow. In this tow, the crack contour is less smooth. Then, it spreads as inter-tow cracking, following the boundary of a tow (see Fig. 5b). The tow is oriented almost perpendicular to the crack itself, but its end is almost parallel. The crack did not spread through the perpendicular tow underneath. It rather evolved as tow debonding (see Fig. 5c), which ended several tens of micrometres lower (see Fig. 5d). This crack did not break the specimen; it unfortunately failed close to the grips in an un-scanned section.

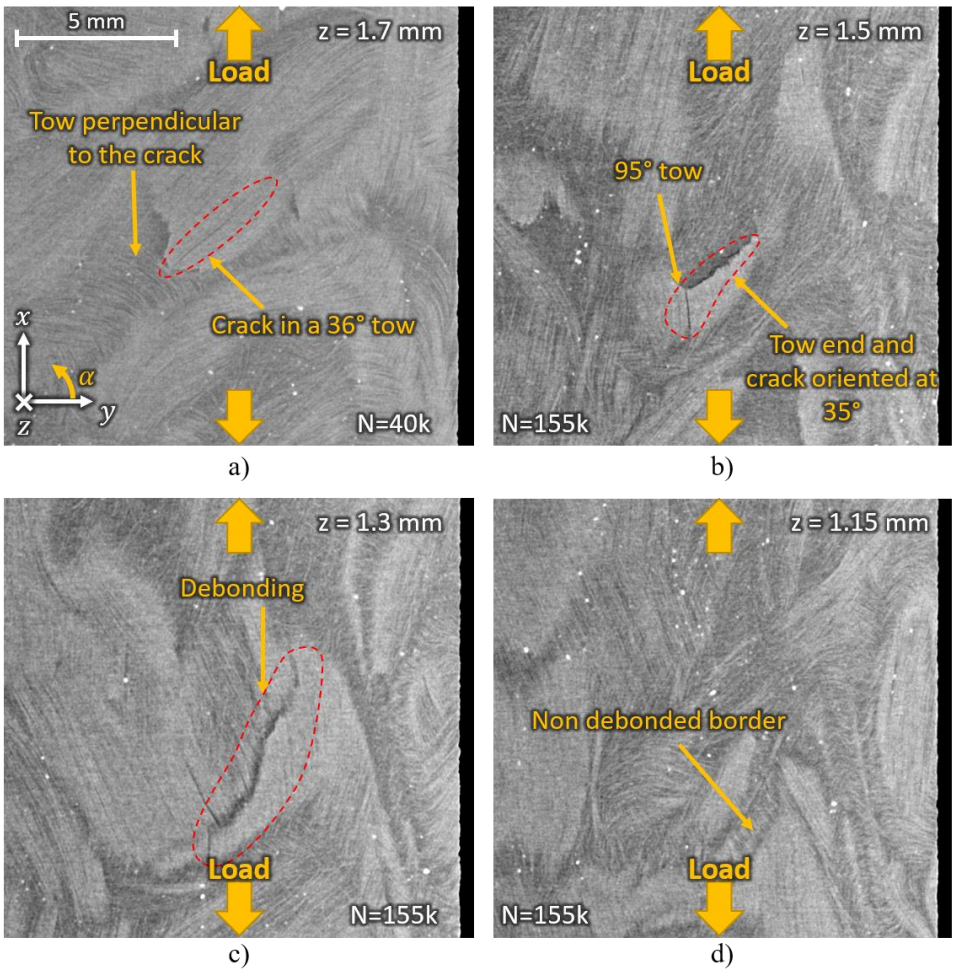


Fig. 5: A small crack in the 0°-A specimen: a) the only visible presence of the crack in the 40k scan, b to d) crack evolution in the 155k scan, at different depths. Load is in the x-direction.

In the same specimen, a larger scale tow debonding was observed and reported in Fig. 6. The debonding's maximum extension in the x- and y-directions was about 13 mm and 10 mm, respectively. The in-plane dimensions of a tow are 25.4 mm by 8 mm; the debonding thus affected more than one tow. In this same specimen, another major crack of similar dimension was observed. Despite their size, neither defect was enough to break the specimen, which failed elsewhere.

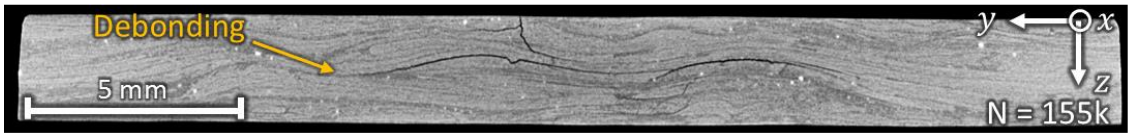


Fig. 6: Debonding of tows observed in the 0°-A specimen. Load is in the x-direction.

A similar crack behaviour was observed in the 0°-B specimen, as shown in Fig. 7. In the outer layer, Fig. 7a reveals the presence of matrix cracks. Those are irregular, and only partially follow the boundary of the tows, as in the skin layer those are highly disrupted [5]. The cracks are observed to merge in a single intra-tow crack when entering the core of the specimen (see Fig. 7b). Deeper down, the crack follows the profile of a similarly oriented tow end (see Fig. 7c), but it does not propagate through a transverse tow (see Fig. 7d). The entire area was crack-free before loading. This crack did not lead the specimen to failure.

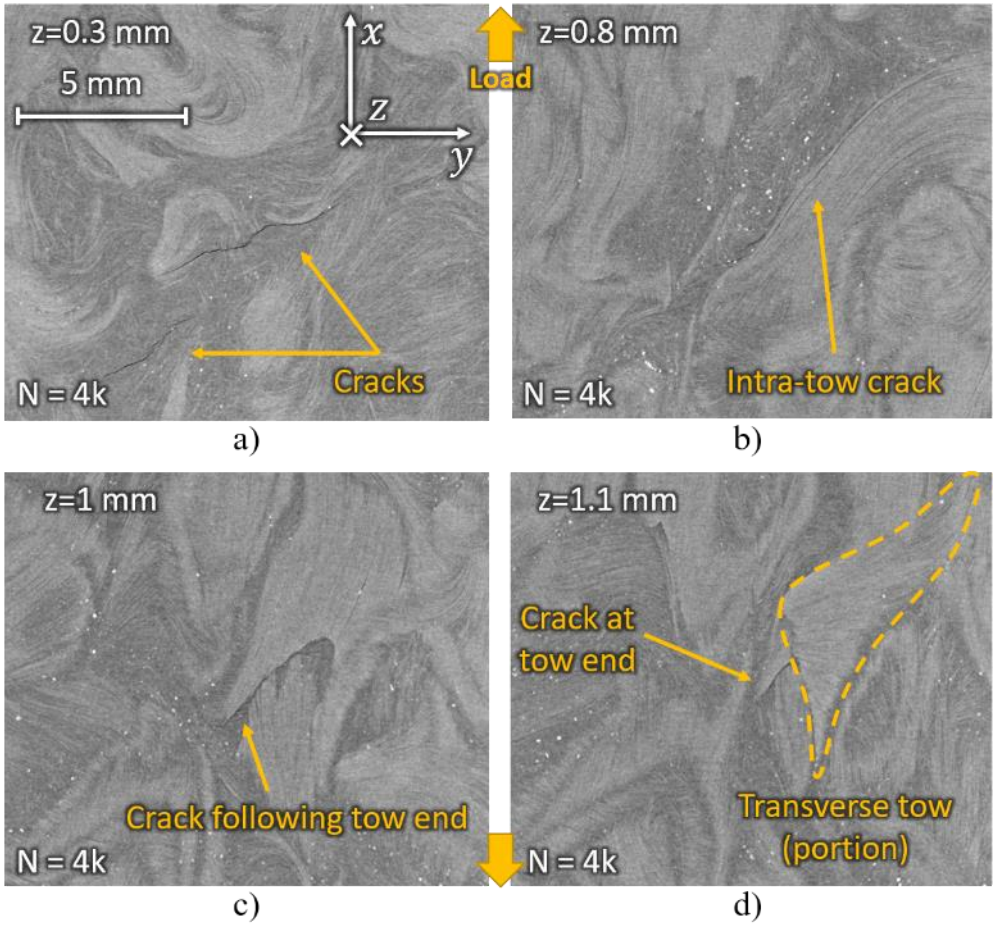


Fig. 7: A crack not leading to failure the specimen 0°B after 4k cycles: a-d) show the same crack at different heights. Loads is in the x-direction.

Fig. 8 shows the cracks leading to failure the 90°-A specimen. The region was intact before testing. Intra-tow cracks develop after only 4k cycles (see Fig. 8a). After 36k cycles (61% of the specimen's life), the cracks spread mainly in the positive z-direction (see Fig. 8b). In Fig. 8c, a curved tow, with a strong y-component, is visible. This tow is not cracked. Below it, the crack is visible in a 12° tow (see Fig. 8d). The crack extents through many tows with similar orientation. When the crack is inside the tows (see Fig. 8d, Fig. 8e and Fig. 8g), it has a smooth contour following the tow orientation, likely involving fibre-matrix debonding and intra-tow matrix cracking. When spreading through the inter-tow matrix-rich zones (see Fig. 8f and Fig. 8h), it has an irregular contour, and often follows the boundaries of nearby tows. The irregular contour

suggests a prevailing inter-tow matrix cracking in the matrix-rich zones in between tows.

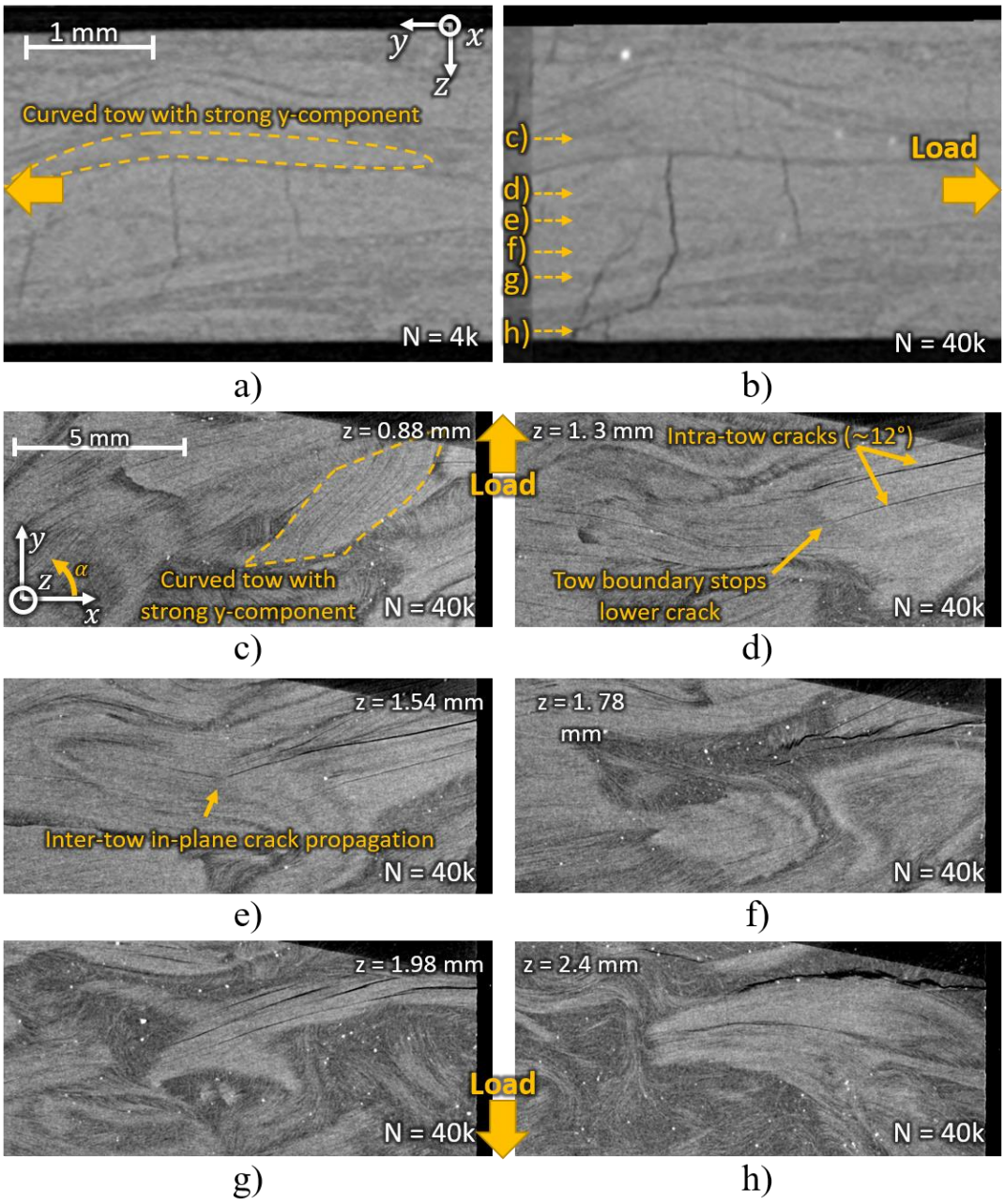


Fig. 8: Cracks leading to failure of specimen 90°-A: a) through-thickness slice after 4k cycles, b) through-thickness slice after 40k cycles, c-h) in-plane slices at different heights of the crack after 40k cycles. Load is in the y-direction.

Another longitudinal section of the same specimen, several tens of mm away from the failure zone analysed earlier, is shown in Fig. 9 at different cycles. No crack was

observed in the pre-test scan in this same location. After 4k cycles, only one crack is seen in Fig. 9a. However, after 40k cycles (see Fig. 9b), a total of 10 cracks are present within a region of about 10 millimetres. Interestingly, the crack observed in the earlier scan did not propagate. It was stopped at the tow boundaries by the upper and lower tows, that were mainly oriented perpendicularly to the crack itself. A new crack formed in the proximity of the first one, in the same tow.

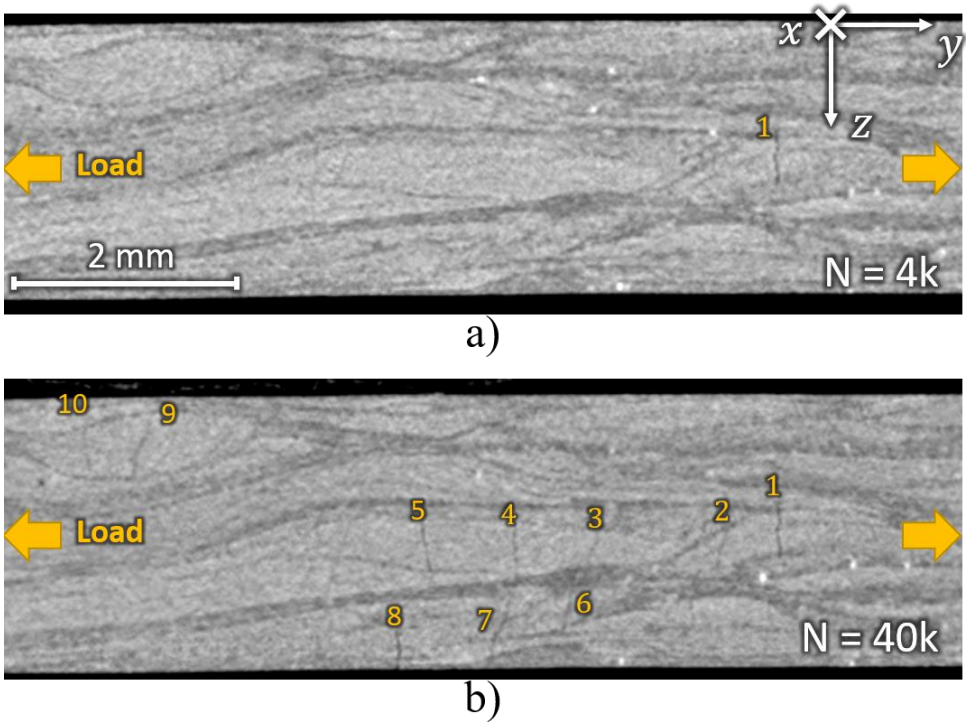


Fig. 9: Crack development in the 90°-A specimen. a) and b) show the same cross section at 4k cycles and at 40k cycles, respectively. The specimen failed at approximately 59K cycles. Load is in the y-direction.

Finally, for all specimens described so far, several defects (voids, cracks and delaminated areas) were observed in the pre-test scans. These were already reported in [5] to have no effect on the final failure of the material in a static tensile test. Here, we confirmed that those defects also did not propagate during cyclic loading. Some examples are shown for the 0° specimens in Fig. 10a and Fig. 10b, and for a 90° specimen in Fig. 10c. Overall, the size of these defects were found to range from about

1 mm to 3 mm, which is comparable to the smaller intra-tow cracks cause by the fatigue loading. Moreover, although significantly smaller than the in-plane dimensions of the tows, they are several times larger than their thickness. Given the highlighted through-the-thickness propagation mechanism, the size of such defects may not be considered negligible. Nevertheless, they do not impact the fatigue life of CF-SMCs. Note that, however, this is not an exclusive feature of CF-SMC: the creation of new crack systems upon fatigue loading was observed for textile composites as well [42]. In addition, considering complex parts, features like corners, section variations or thick-walled designs can result in larger manufacturing defects. In [43], µCT scans revealed the presence of significantly larger manufacturing defects (up to 30 mm) on a thick-walled part. Considering such defect size, it is reasonable to assume that they might impact the part fatigue life. More experimental evidence is needed for a definitive answer.

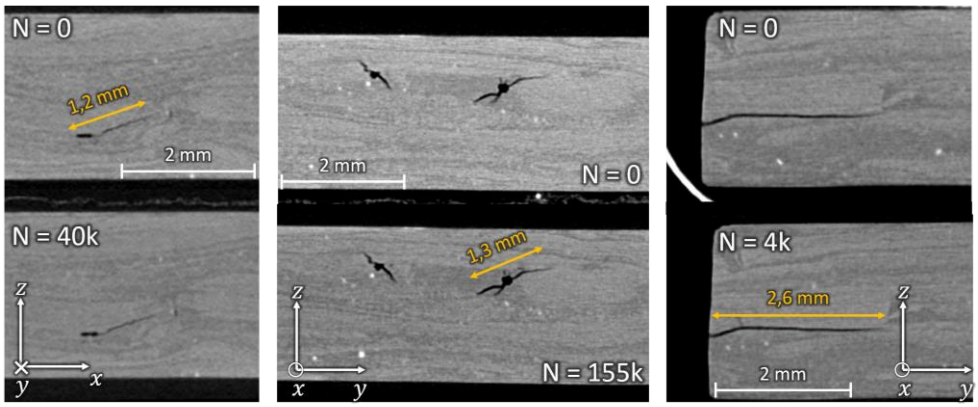


Fig. 10: Examples of non-propagating pre-existent manufacturing defects in the a) 0°-B, b) 0°-A and c) 90°-A specimens.

4 Discussion

4.1 Damage and crack arrest mechanisms

The pre-failure scans revealed the presence of intra-tow splitting, following the tow orientation, as common damage mechanism for both 0° and 90° specimens. As shown in section 3.2, this was the first fatigue damage mode to develop in the specimens. Those splits followed the longitudinal axis of the tows: together with the smooth crack contour, this suggests a combination of fibre-matrix debonding and matrix cracking, with no fibre failure.

The intra-tow cracks have two possible propagation directions with respect to the tow they nucleate into. The first one is the in-plane direction parallel to the tow axis, or the 1-axis direction in Fig. 11. The second one is the through-the-thickness propagation, or the 3-axis direction in Fig. 11. The in-plane direction perpendicular to the tow axis (2-axis direction in Fig. 11) is clearly prevented by the tow itself, as it would require significant fibre breakage.

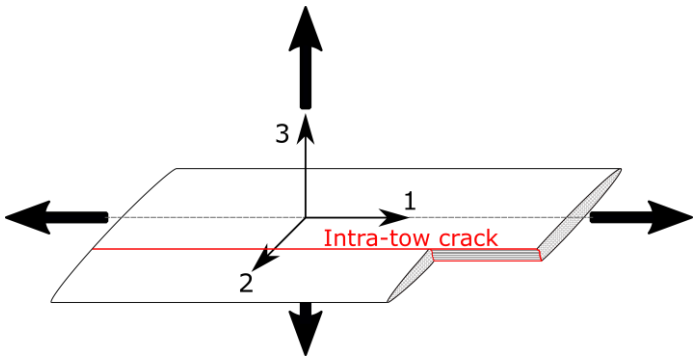


Fig. 11: Possible directions for the crack propagation outside the tow.

The in-plane propagation (along the 1-axis of the tow) requires the presence of another tow close to the boundary of the crack initiating tow. Moreover, both tows must have a similar orientation. When those conditions are not met, the in-plane propagation is

prevented (see Fig. 5a). If those conditions are verified, the crack can spread into the neighbouring tow, as shown in Fig. 8e. However, it must be pointed out that, in this case, both tows will be oriented in a favourable direction for cracks to nucleate. Whether the crack grows from one tow into the other, or simply the creation of two independent cracks which eventually coalesce, cannot be derived from the presented results. Moreover, Fig. 8d shows a crack that did not even spread between two similarly oriented tows, revealing that similar tow orientation is a necessary but not a sufficient condition. Given the debonding nature of the intra-tow crack, when the fibre ends, the crack must change its propagation mechanism: either it spreads in an inter-tow matrix pocket or it spreads in a tow with a similar orientation. However, these new propagating mechanisms might require more energy than that required to the crack to nucleate and spread along a fibre interface; Fig. 7d suggests that even spreading to an adjacent tow with similar orientation may be not as easy for the crack. In such sense, the end of the tows act as a barrier for inter-tow in-plane propagation of intra-tow cracks. A slow in-plane crack propagation, up until crack arrest, was already observed in [44,45].

Through-the-thickness propagation was more commonly observed. Along this direction, the crack still tries to maintain its orientation. This is possible only by spreading to a similarly oriented tow or in the matrix along similarly oriented tow boundaries (see Fig. 5b and Fig. 7c). When perpendicularly oriented tows are met by an advancing crack front, the crack is stopped. This is clearly visible in Fig. 8b for the crack breaking the specimen, but also in Fig. 9: here, the numerous nucleated cracks were all confined within a few tows. The only crack in Fig. 9a observed in the early life scan did not propagate, but rather another one formed in the same tow.

In the 0°-A specimen some cracks were not stopped immediately by perpendicularly oriented tows, but rather evolved into tow debonding. In the case of Fig. 5, the debonding stopped after about 150 μm. The transition to debonding implies a transition from mode I to mainly mode II. This probably explains why the crack was stopped. For the case of Fig. 6, instead, the debonding grew quite large in size, but still did not bring the specimen to failure. Overall, this failure mode was found to be not critical.

Two major cracks (>10 mm) where observed only in the 0°-A specimen (one is the debonding observed in Fig. 6). Their morphology was strongly affected by the presence and orientation of the tows, confirming their effects on the fatigue crack growth. Moreover, the specimen failed in neither of the two defects, confirming the low defect or notch sensitivity of this material [5,46–48].

The proposed failure mechanism can be used to explain the dynamics of the crack in the 0°-B specimen reported in Fig. 7. The crack likely nucleates inside the tow of Fig. 7b, and then propagates through-the-thickness in both directions, reaching the outer surface upward (see Fig. 7a). In the opposite direction, it spreads first through a tow boundary (see Fig. 7c) and then it is stopped by a transversely oriented tow (see Fig. 7d).

The 90°-A specimen showed a higher presence of intra-tow cracks in the tows oriented perpendicularly to the load (see Fig. 8a, Fig. 8b Fig. 9b). This is reasonable, as those tows are mainly loaded in mode I. Very few of those cracks, however, were able to spread through the adjacent tows.

Overall, it was shown how the morphology of SMC tends to arrest fatigue cracks. Many of these cracked areas proved to be very stable, not leading to failure the material. Failure happened when several of these areas were concentrated in a small region. Due

to this increasing crack concentration, the remaining intact cross-section is progressively reduced so that it is not able anymore to withstand the applied load.

Finally, note that the µCT technique allows the observation of several regions within each specimens. The damage mechanisms were described using few examples, but they were commonly observed in different areas of all the scanned specimens. Therefore, it is unlikely that the crack arresting mechanism observed is peculiar to the few lucky specimens we tested. The nature of this mechanism was found to be intrinsic of the morphology of the material, that is similar for all specimens (see also the scanned specimens tested statically in [5]).

4.2 On the fracture surfaces of the specimens

Fig. 3 shows the typical fracture surfaces of each specimens group, for both the static and fatigue case. Considering the failure dynamic highlighted with the µCT scans, further observations can be made.

First, while no tow breakage was caused by the fatigue loading, some broken tows were present in the fracture surface of the specimens, especially the 0° ones. It is thus likely that those tows were broken in the final static failure of the remaining surface.

The angle of the failure profile of the 45° and 90° specimens, on the contrary, can be related to the fatigue damage mechanisms described earlier. As explained in the previous section, the damage likely nucleates inside the tows; a preferential orientation state implies that the number of tows oriented at a certain angle is statistically higher. Therefore, the number of intra-tow cracks oriented at the same orientation will also be higher. It was also observed that the propagation of said cracks is overall preserved. It is

thus reasonable to explain the similarity between the preferential orientation of the specimens and the angle of their fracture surface.

This theory, however, assumes that the nucleation of intra-tow cracks is not affected by the orientation of those tows. The statistical similarity of the SN curves supports such assumption, although a definitive confirmation cannot be given only based on the present work. However, doubts can be raised mainly in the case of the 0° case, while it is reasonable to assume that the difference between the 45° and 90° is minor.

4.3 Performance comparison with other composites

In Fig. 12, the normalised CF-SMC curves are compared with others reported in the literature for other TBDCs [11,14,49], SFRPs [19,20,23,24] and a QI laminate [11], all tested with the same R-ratio.

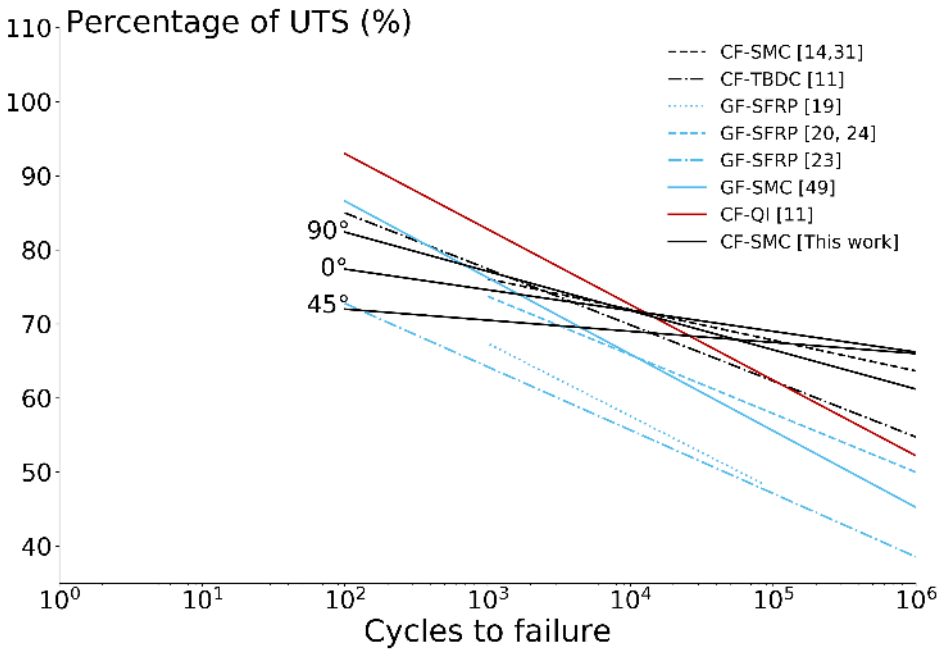


Fig. 12: Comparison of SN curves from different composite systems. Black lines refer to carbon TBDCs, light blue lines to glass composites (both SFRP and SMC) and red line is for QI laminate. CF and GF distinguish carbon and glass fibres, respectively.

The CF-SMC curves obtained in the present are close to the one of a similar material reported in [14]. Those two CF-SMCs have the same tow length (25 mm), similar volume fraction (42% against 40%), but the global orientation in the result from the literature is random isotropic [14]. The similarities between those curves confirms the small influence of the global orientation on the normalised fatigue performance observed in section 3.1.

Interestingly, carbon TBDCs curves show a flatter slope than most of the other curves, which suggests that the former are less affected by cyclic loading. In the high-cycle region (>10k cycles), all CF-SMC curves are located higher than the other composites considered, including the QI laminate curve. The glass SMC curve is halfway between the carbon TBDC and the SFRPs curves.

4.4 Contributions to the state of the art

In contrast with the state of the art, this investigation focused on CF-SMC with a prevailing fibre orientation resulting from a high in-mould flow moulding. The orientation of the tows proved significant in the determination of the different SN curves. However, it had no significant effect on the normalised SN curves, also considering the curve for a similar randomly oriented CF-SMC presented in [14,31]. The statistical similarity between all considered curves can be thus used in the preliminary design against fatigue of parts, when only the SN curve of a single orientation and the static data of all the orientations are available.

Moreover, this work proposes a new theory for the fatigue damage mechanisms happening in TBDCs. This theory includes all the different phases of the life of the material: (1) nucleation as intra-tow phenomenon, (2) propagation through the matrix

layers, tow boundaries or inside other tows, and (3) final static failure of the remaining section. In addition, these failure development did not seem not to depend on the tow orientation.

Finally, the proposed theory implies the existence of a crack arresting mechanism caused by the heterogeneous microstructure. An explanation for the relatively flat slope of the SN curves of TBDCs is proposed for the first time.

5 Conclusions

The present work presented the results of a fatigue investigation on CF-SMC, using both mechanical testing and μCT scans. Particular attention was given to the influence of tow orientations on the fatigue performance of the material: the obtained SN diagrams depended on the prevailing tow orientation. However, upon normalisation with the relative static UTS, the curves collapsed into a single master curve. The damage evolution analysis highlighted the presence of a crack arresting mechanism induced by the material morphology.

First, nucleation involves intra-tow splitting, as combination of fibre-matrix debonding and matrix cracking, irrespectively of the local tow orientation. After this nucleation and intra-tow propagation, the cracks tend to propagate mainly in the through-the-thickness direction preserving their original orientation. This can be possible when similarly oriented tows or tow ends are found along the crack path. Perpendicularly oriented tows, instead, arrest the cracks. Since those defects can no longer propagate, new ones are formed and undergo a similar process. The reduction of a resistant cross-section by several cracks closely located causes the final failure, instead of the nucleation and propagation of a single defect.

The normalised SN curves were compared with other normalised SN curves of other composites: the slope of the CF-SMC curves was flatter than the other considered composites and, for fatigue lives longer than 10k cycles, located at higher percentage of the UTS. After 1 million cycles, CF-SMC could still withstand more than 65% of its UTS.

This work suggested the existence of a morphological fatigue crack arresting mechanism in CF-SMC. This makes such materials very suitable for high-cycle fatigue application. The presented work is thus a further step in the wide-spread adoption of CF-SMC in fatigue-driven applications, such as automotive components.

6 Acknowledgments

The research leading to these results has been performed within the framework of the FiBreMoD project and has received funding from the European Union's Horizon 2020 research and innovation programme under the Marie Skłodowska-Curie grant agreement No 722626. YS acknowledges FWO Flanders for his postdoctoral fellowship. SVL holds the Toray Chair at KU Leuven, the support of which is acknowledged. SP acknowledges her Research Fellowship of the Royal Academy of Engineering on "Multiscale discontinuous composites for high-volume and sustainable applications" (2015-2019). The authors acknowledge Mitsubishi Chemical Carbon Fiber and Composites GmbH for providing material and related information. The micro-CT images have been acquired on the X-ray computed tomography facilities at KU Leuven, maintained under the supervision of Prof M. Wevers and financed by the Hercules Foundation and the Research Council of KU Leuven (project C24/17/052); help of Dr. Jeroen Soete and of Johan Vanhulst is gratefully acknowledged. Bart

Pelgrims is acknowledged for his help with the fatigue tests. LMM acknowledges Mariangela Panzarino (Thermo Fisher Scientific) for her useful suggestions on the statistical analysis.

7 References

[1] Han CD. Rheology and Processing of Polymeric Materials, Volume 1: Polymer Rheology. USA: Oxford University Press; 2007.
[2] Visweswaraiah SB, Selezneva M, Lessard L, Hubert P. Mechanical characterisation and modelling of randomly oriented strand architecture and their hybrids – A general review. J Reinf Plast Compos 2018;37:548–80.
[3] Wan Y, Takahashi J. Tensile properties and aspect ratio simulation of transversely isotropic discontinuous carbon fiber reinforced thermoplastics. Compos Sci Technol 2016;137:167–76.
[4] Wan Y, Takahashi J. Tensile and compressive properties of chopped carbon fiber tapes reinforced thermoplastics with different fiber lengths and molding pressures. Compos Part A Appl Sci Manuf 2016;87:271–81.
[5] Martulli LM, Muyshondt L, Kerschbaum M, Pimenta S, Lomov S V, Swolfs Y. Carbon fibre sheet moulding compounds with high in-mould flow: Linking morphology to tensile and compressive properties. Compos Part A Appl Sci Manuf 2019;126:105600.
[6] Nicoletto G, Riva E, Stocchi A. Mechanical Characterization of Advanced Random Discontinuous Carbon/Epoxy Composites. Mater Today Proc 2016;3:1079–84.
[7] Denos BR, Kravchenko SGS, Pipes RB. Progressive Failure Analysis in Platelet Based Composites Using CT-Measured Local Microstructure. Int. SAMPE Tech. Conf., Seattle (WA): 2017.
[8] Johanson K, Harper LT, Johnson MS, Warrior NA. Heterogeneity of discontinuous carbon fibre composites: Damage initiation captured by Digital Image Correlation. Compos Part A Appl Sci Manuf 2015;68:304–12.
[9] Piry M, Michaeli W. Stiffness and failure analysis of SMC components considering the anisotropic material properties. Macromol Mater Eng 2000;284–285:40–5.
[10] Li Y, Pimenta S, Singgih J, Nothdurfter S, Schuffenhauer K. Experimental investigation of randomly-oriented tow-based discontinuous composites and their equivalent laminates. Compos Part A Appl Sci Manuf 2017;102:64–75.
[11] Selezneva M, Lessard L. Characterization of mechanical properties of randomly oriented strand thermoplastic composites. J Compos Mater 2016;50:2833–51.
[12] Evans AD, Qian CC, Turner TA, Harper LT, Warrior NA. Flow characteristics of carbon fibre moulding compounds. Compos Part A Appl Sci Manuf 2016;90:1–12.
[13] Feraboli P, Peitso E, Cleveland T, Stickler PB. Modulus Measurement for Prepreg-based Discontinuous Carbon Fiber/Epoxy Systems. J Compos Mater 2009;43:1947–65.
[14] Tang H, Chen Z, Zhou G, Sun X, Li Y, Huang L, et al. Effect of fiber orientation

distribution on constant fatigue life diagram of chopped carbon fiber chip-reinforced Sheet Molding Compound (SMC) composite. Int J Fatigue 2019;125:394–405.
[15] Feraboli P, Peitso E, Deleo F, Cleveland T, Stickler PB. Characterization of Prepreg-Based Discontinuous Carbon Fiber / Epoxy Systems. J Reinf Plast Compos 2009;28:1191–214.
[16] Steinwolf A, Giacomin JA, Staszewski WJ. On the need for bump event correction in vibration test profiles representing road excitations in automobiles. Proc Inst Mech Eng Part D J Automob Eng 2002;216:279–95.
[17] Mortazavian S, Fatemi A. Fatigue behavior and modeling of short fiber reinforced polymer composites: A literature review. Int J Fatigue 2015;70:297–321.
[18] Carvelli V, Jain A, Lomov S. Fatigue of Textile and Short Fiber Reinforced Composites. UK: John Wiley & Sons; 2017.
[19] Bernasconi A, Davoli P, Basile A, Filippi A. Effect of fibre orientation on the fatigue behaviour of a short glass fibre reinforced polyamide-6. Int J Fatigue 2007;29:199–208.
[20] Zhou Y, Mallick PK. Fatigue performance of an injection-molded short E-glass fiber-reinforced polyamide 6,6. I. Effects of orientation, holes, and weld line. Polym Compos 2006;27:230–7.
[21] Guster C, Pinter G, Mösenbacher A, Eichlseder W. Evaluation of a simulation process for fatigue life calculation of short fibre reinforced plastic components. Procedia Eng 2011;10:2104–9.
[22] Brunbauer J, Mösenbacher A, Guster C, Pinter G. Fundamental influences on quasistatic and cyclic material behavior of short glass fiber reinforced polyamide illustrated on microscopic scale. J Appl Polym Sci 2014;131:1–14.
[23] Jain A, Veas JM, Straesser S, Van Paepegem W, Verpoest I, Lomov S V. The Master SN curve approach – A hybrid multi-scale fatigue simulation of short fiber reinforced composites. Compos Part A Appl Sci Manuf 2016;91:510–8.
[24] De Monte M, Moosbrugger E, Quaresimin M. Influence of temperature and thickness on the off-axis behaviour of short glass fibre reinforced polyamide 6.6 - Cyclic loading. Compos Part A Appl Sci Manuf 2010;41:1368–79.
[25] Wyzgoski MG, Krohn JA, Novak GE. Fatigue of fiber-reinforced injection molded plastics. I: Stress-lifetime data. Polym Compos 2004;25:489–98.
[26] Horst JJ, Spoormaker JL. Mechanisms of fatigue in short glass fiber reinforced polyamide 6. Polym Eng Sci 1996;36:2718–26.
[27] Klimkeit B, Castagnet S, Nadot Y, Habib A El, Benoit G, Bergamo S, et al. Fatigue damage mechanisms in short fiber reinforced PBT+PET GF30. Mater Sci Eng A 2011;528:1577–88.
[28] Arif MF, Saintier N, Meraghni F, Fitoussi J, Chemisky Y, Robert G. Multiscale fatigue damage characterization in short glass fiber reinforced polyamide-66. Compos Part B Eng 2014;61:55–65.
[29] Mallick PK. Fatigue Characteristics of High Glass Content Sheet Molding Compound (SMC) Materials. Polym Compos 1981;2:18–21.
[30] Ben Cheikh Larbi A, Sai K, Sidhom H, Baptiste D. Constitutive model of micromechanical damage to predict reduction in stiffness of a fatigued SMC composite. J Mater Eng Perform 2006;15:575–80.
[31] Tang H, Zhou G, Chen Z, Huang L, Avery K, Li Y, et al. Fatigue behavior

analysis and multi-scale modelling of chopped carbon fiber chip-reinforced composites under tension-tension loading condition. Compos Struct 2019;215:85–97.
[32] Garcea SC, Wang Y, Withers PJ. X-ray computed tomography of polymer composites. Compos Sci Technol 2018;156:305–19.
[33] Garcea SC, Sinclair I, Spearing SM. In situ synchrotron tomographic evaluation of the effect of toughening strategies on fatigue micromechanisms in carbon fibre reinforced polymers. Compos Sci Technol 2015;109:32–9.
[34] Garcea SC, Sinclair I, Spearing SM. Fibre failure assessment in carbon fibre reinforced polymers under fatigue loading by synchrotron X-ray computed tomography. Compos Sci Technol 2016;133:157–64.
[35] Nixon-Pearson OJ, Hallett SR, Withers PJ, Rouse J. Damage development in open-hole composite specimens in fatigue. Part 1: Experimental investigation. Compos Struct 2013;106:882–9.
[36] Yu B, Blanc R, Soutis C, Withers PJ. Evolution of damage during the fatigue of 3D woven glass-fibre reinforced composites subjected to tension–tension loading observed by time-lapse X-ray tomography. Compos Part A Appl Sci Manuf 2016;82:279–90.
[37] Mitsubishi Chemical Corporation. Pyrofil STR120 Datasheet 2016.
[38] Mitsubishi Chemical Corporation. TR50s Datasheet 2012.
[39] ASTM D3479. Standard Test Method for Tension-Tension Fatigue of Polymer Matrix Composite. vol. 08. 2002.
[40] Shneider CRA, Maddox SJ. Best Practice Guide on Statistical Analysis of Fatigue Data. 2003.
[41] ASTM E739. Standard Practice for Statistical Analysis of Linear or Linearized Stress-Life (S-N) and Strain-life (ε-N) Fatigue Data. 2004.
[42] Karahan M, Lomov S V., Bogdanovich AE, Verpoest I. Fatigue tensile behavior of carbon/epoxy composite reinforced with non-crimp 3D orthogonal woven fabric. Compos Sci Technol 2011;71:1961–72.
[43] Martulli LM, Creemers T, Schöberl E, Hale N, Kerschbaum M, Lomov S V., et al. A thick-walled sheet moulding compound automotive component: Manufacturing and performance. Compos Part A Appl Sci Manuf 2020;128:105688.
[44] Tiefenthaler M, Stelzer PS, Chung CN, Reisecker V, Major Z. Characterization of the Fracture Mechanical Behavior of C-Smc Materials. Acta Polytech CTU Proc 2018;18:1.
[45] Boursier B, Lopez A. Failure Initiation and Effect of Defects in Structural Discontinuous Fiber Composites. Soc Adv Mater Process Eng 2010.
[46] Qian C, Harper L, Turner TA, Warrior NA. Notched behaviour of discontinuous carbon fibre composites: Comparison with quasi-isotropic non-crimp fabric. Compos Part A Appl Sci Manuf 2011;42:293–302.
[47] Feraboli P, Peitso E, Cleveland T, Stickler PB, Halpin JC. Notched behavior of prepreg-based discontinuous carbon fiber/epoxy systems. Compos Part A Appl Sci Manuf 2009;40:289–99.
[48] Pimenta S, Ahuja A, Lau AY. Damage Tolerant Tow-Based Discontinuous Composites. 20th Int. Conf. Compos. Mater., Copenhagen, Denmark: 2015.
[49] Laribi MA, Tamboura S, Fitoussi J, Tié Bi R, Tcharkhtchi A, Ben Dali H. Fast fatigue life prediction of short fiber reinforced composites using a new hybrid

damage approach: Application to SMC. Compos Part B Eng 2018;139:155–62.

View publication stats